HEALTH AND MEDICINE

Transgene-free remote magnetothermal regulation of adrenal hormones

Dekel Rosenfeld[1], Alexander W. Senko[1,2], Junsang Moon[1,2], Isabel Yick[3], Georgios Varnavides[1,2,4], Danijela Gregurec[1], Florian Koehler[1,5], Po-Han Chiang[1], Michael G. Christiansen[6], Lisa Y. Maeng[7], Alik S. Widge[7]*†, Polina Anikeeva[1,2,8]†

The field of bioelectronic medicines seeks to modulate electrical signaling within peripheral organs, providing temporally precise control of physiological functions. This is usually accomplished with implantable devices, which are often unsuitable for interfacing with soft and highly vascularized organs. Here, we demonstrate an alternative strategy for modulating peripheral organ function, which relies on the endogenous expression of a heat-sensitive cation channel, transient receptor potential vanilloid family member 1 (TRPV1), and heat dissipation by magnetic nanoparticles (MNPs) in remotely applied alternating magnetic fields. We use this approach to wirelessly control adrenal hormone secretion in genetically intact rats. TRPV1-dependent calcium influx into the cells of adrenal cortex and medulla is sufficient to drive rapid release of corticosterone and (nor)epinephrine. As altered levels of these hormones have been correlated with mental conditions such as posttraumatic stress disorder and major depression, our approach may facilitate the investigation of physiological and psychological impacts of stress.

INTRODUCTION

The hypothalamic-pituitary-adrenal (HPA) axis is the primary neuroendocrine axis that regulates the stress response in mammals (*1*). Dysregulation of the HPA axis and the adrenal gland has been linked to mental conditions including depression, posttraumatic stress disorder, metabolic dysfunction, and anxiety (*2*). The ability to control the release of adrenal hormones with temporal precision may empower studies of stress biology and advance therapeutic approaches for stress-related mental illnesses (*3*).

Modulation of electroactive peripheral organ tissues, such as adrenal glands, with the goal of regulating their function can be accomplished by interfacing either with the end organ directly or with its peripheral innervation (*4*). Currently, peripheral organ modulation relies on mechanically invasive implanted electrodes (*5*), which pose challenges to chronic interfacing with small, soft, and densely vascularized organs. The adoption of techniques that rely on electromagnetic induction (*6*), acoustic (*7*), or optical (*8*) signals is hindered by tissue absorption and scattering, limited spatial resolution, or reliance on transgenes. Weak alternating magnetic fields (AMFs) with frequencies of hundreds of kilohertz can penetrate deep into the body with no attenuation or deleterious physiological effects. Coupled to heat dissipation by magnetic nanoparticles (MNPs), these AMFs offer an attractive means to deliver signals to deep tissues, a phenomenon exploited extensively in cancer hyperthermia (*9*) and recently leveraged to control cell signaling (*10*, *11*), gene expression (*12*), drug delivery (*13*), and animal behavior (*14*). To date, the magnetothermal strategy for control of physiological functions has relied on exogenously delivered transgenes, including the heat-sensitive cation channel transient receptor potential vanilloid family member 1 [TRPV1, the capsaicin (CAP) receptor] to mediate transduction of thermal stimuli into changes in cell membrane potential (*11*). The robust endogenous expression of TRPV1 across the peripheral nerves and organs (*15*) suggests the possibility of applying magnetothermal control to remotely modulate organ function without reliance on transgenes.

Here, we test this hypothesis by developing a magnetothermal switch for on-demand release of the adrenal hormones epinephrine and corticosterone. These hormones are produced by the adrenal medulla (*16*) and cortical zona fasciculata (ZF) (*17*), respectively, and their secretion is dependent on intracellular calcium (Ca^{2+}) concentration (Fig. 1A) (*16*, *18*, *19*). Notably, mRNA profiling studies demonstrate robust expression of TRPV1 in the adrenal glands of rabbits and rats (*15*, *20*). Therefore, we reasoned that remotely delivered magnetothermal stimuli may trigger Ca^{2+}-permeable TRPV1 channels in the cells of adrenal medulla and ZF allowing for temporally precise control of adrenal hormones (Fig. 1B). This approach may advance the fundamental study of the HPA axis in stress-related disorders while simultaneously offering a generalizable strategy to modulating peripheral organ function.

RESULTS

TRPV1 expression in the adrenal gland

We corroborated the expression of TRPV1 throughout the rat adrenal gland via immunohistochemistry (Fig. 1, C to H). We found that 35% of cells in the adrenal medulla and 20% in the adrenal cortex express this cation channel. In the adrenal medulla, we observed an overlap of TRPV1 with the synaptic protein synaptophysin (SYN) (*21*), suggesting the presence of this receptor at the synaptic terminals of the splanchnic

[1]Research Laboratory of Electronics and McGovern Institute for Brain Research, Massachusetts Institute of Technology, Cambridge, MA 02139, USA. [2]Department of Materials Science and Engineering, Massachusetts Institute of Technology, Cambridge, MA 02139, USA. [3]Department of Biology, Wellesley College, Wellesley, MA 02481, USA. [4]John A. Paulson School of Engineering and Applied Sciences, Harvard University, Cambridge, MA 02139, USA. [5]Department of Electrical Engineering and Computer Science, Massachusetts Institute of Technology, Cambridge, MA 02139, USA. [6]Department of Health Sciences and Technology at the Swiss Federal Institute of Technology in Zürich (ETHZ), Zürich 8093, Switzerland. [7]Division of Neurotherapeutics, Massachusetts General Hospital and Department of Psychiatry, Harvard Medical School, Charlestown, MA 02129, USA. [8]Department of Brain and Cognitive Sciences, Massachusetts Institute of Technology, Cambridge, MA 02139, USA.
*Present address: Department of Psychiatry, University of Minnesota, Minneapolis, MN 55455, USA.
†Corresponding author. Email: anikeeva@mit.edu (P.A.); awidge@umn.edu (A.S.W.)

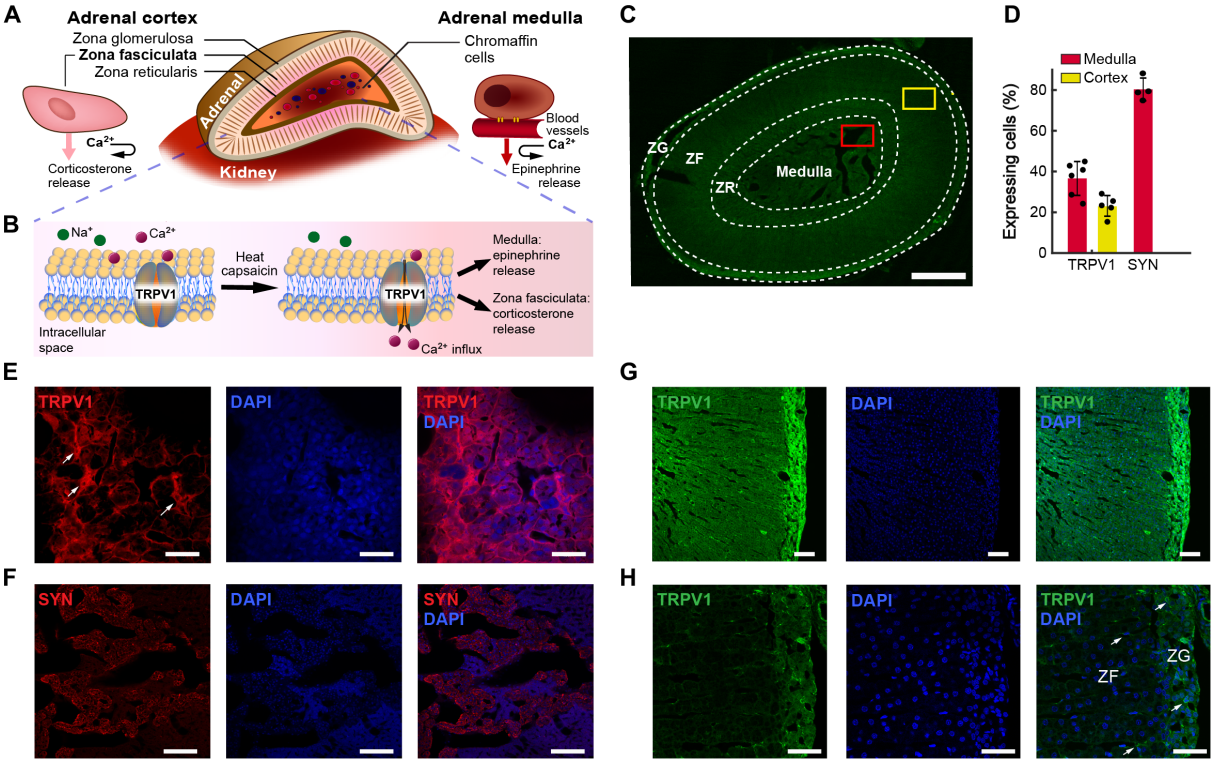

Fig. 1. TRPV1 expression in the adrenal gland. (**A**) Adrenal gland anatomy: The chromaffin cells of the medulla secrete epinephrine and norepinephrine. The ZF cells of the adrenal cortex secrete corticosterone. Both processes are Ca^{2+} dependent. (**B**) An illustration of Ca^{2+} influx through TRPV1 channels in response to heat or CAP. (**C**) TRPV1 expression in the rat adrenal gland visualized via immunofluorescence across the different zones. Scale bar, 500 μm. The zona reticularis (ZR) in rats functions similarly to the ZF. The red and yellow squares indicate locations of immunoanalysis of TRPV1 expression in the medulla (**E** and **F**) and ZF (**G** and **H**), respectively. (**D**) Quantification of TRPV1 and SYN expression and in the adrenal medulla and cortex [$n = 4$ to 6, means ± standard deviation (std.)] (E and F) Immunofluorescence images of TRPV1 (E) (red) and SYN (F) (red) in the medulla. (G and H) Immunofluorescence images of TRPV1 (green) in ZF. (H) Higher magnification of (G). (E to H) The nuclear stain DAPI is shown in blue. Scale bars, 50 μm.

nerve fibers (Fig. 1F and fig. S1) (*16*). In addition, in the adrenal medulla, we found partial colocalization of TRPV1 with a calcitonin gene-related peptide (CGRP; fig. S1). CGRP is stored in sensory nerve terminals and is associated with pain perception, inflammatory response, and enhanced catecholamine secretion from the adrenal medulla (*22*).

Nanoparticles synthesis and characterization

To assert that the hysteretic heating of MNPs is necessary and sufficient to trigger Ca^{2+} influx into TRPV1-expressing adrenal cells, two sets of ~22-nm chemically inert iron oxide nanoparticles (NPs) were synthesized (*23*). Magnetite (Fe_3O_4, MNP) and wüstite (FeO, WNP) NPs largely share elemental composition yet exhibit distinct crystal structures resulting in vastly different magnetic properties (Fig. 2, A and B). Magnetite has an inverse spinel structure, which yields ferrimagnetic properties with high saturation magnetization and size-dependent coercivity (*24*). In contrast, wüstite exhibits the rock salt structure and is weakly paramagnetic at physiological temperatures (weakly antiferromagnetic below ~200 K) (*25*), which is manifested in low magnetization and negligible coercivity as compared to magnetite (Fig. 2, C and D). Both types of NPs are produced in nearly identical organometallic syntheses, which differ by the ratios of solvents that bias the synthesis toward a more oxidized magnetite or a more reduced wüstite phase (*23*). Following synthesis, both MNPs and WNPs are decorated with hydrophobic oleic acid ligands. To ensure their biocompatibility and solubility in physiological fluids, NPs were functionalized with poly(ethylene glycol) (PEG) with controlled thickness using intercalation of an amphiphilic poly(maleic anhydride-alt-1-octadecene) (PMAO) block within the PEG-PMAO copolymer (Fig. 2, A and B). Minimal internalization of MNPs [~11.6 ± 3.1% of all examined cells, means ± standard deviation (SD)] into adrenal cells was observed following a 24-hour incubation with fluorescently labeled rhodamine-MNPs, as quantified via confocal microscopy and fluorescence intensity measured by a plate reader (fig. S2). Powder x-ray diffraction spectra corroborate the inverse spinel and rock salt phases of MNPs and WNPs, respectively (Fig. 2E). Upon exposure to AMF with an amplitude $H = 15$ kA/m and frequency $f = 515$ kHz, MNPs dissipate heat with specific loss power (SLP; heating efficiency per gram of iron) of 880 ± 38 $W/g_{[Fe]}$ (means ± SD), calorimetrically evaluated using an AMF coil driven by a resonant circuit. The same conditions applied to WNPs yield a negligible SLP of 8 ± 4 W/g (Fig. 2F). Moreover, the magnetic properties of the MNPs were not significantly altered following incubation under physiological conditions, suggesting their applications in long-term in vivo studies (fig. S2).

Calcium influx in adrenal cell culture

Magnetothermal modulation of adrenal function was first evaluated using Ca^{2+} imaging in a primary rat mixed adrenal culture mediated by the heat-sensitive TRPV1 ion channel (Fig. 3, A and B). Cells isolated from adrenal glands remained viable for up to 10 days in vitro even

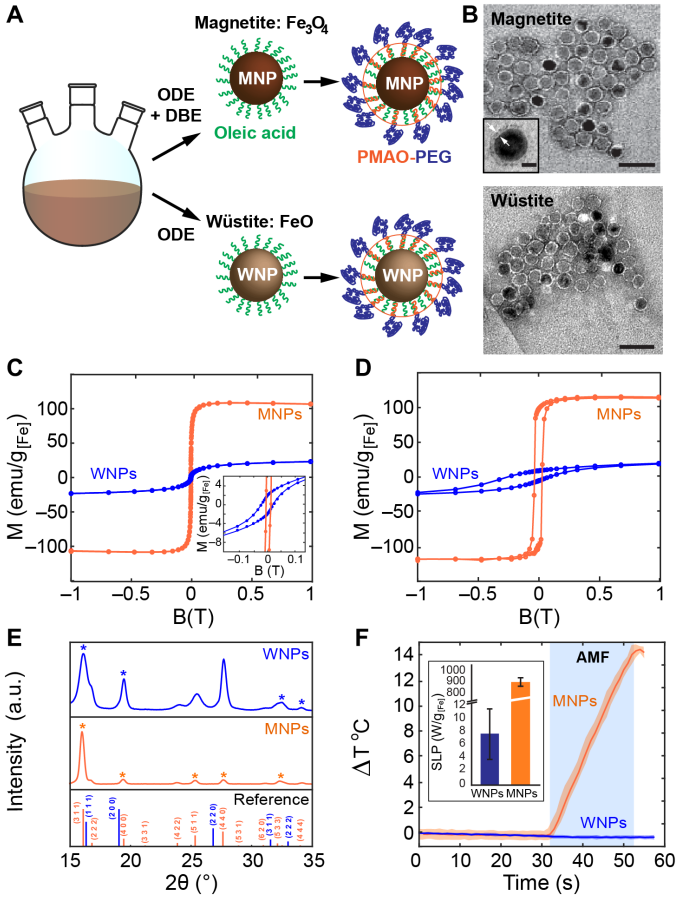

Fig. 2. MNP and WNP synthesis and characterization. (**A**) Organometallic synthesis of MNPs and WNPs in 1-octadecene (ODE) and dibenzyl ether (DBE) mixture or ODE alone, respectively. The NPs are rendered hydrophilic via surface intercalation of PMAO-PEG into the oleic acid coating. (**B**) Transmission electron microscope (TEM) images of MNPs (top) and WNPs (bottom). The bright surface layer corresponds to the PMAO-PEG coating (~2-nm thickness as shown in the inset. Inset scale bar, 10 nm). Scale bars, 50 nm. (**C**) Room temperature magnetization curves and the coercive field measured for MNPs and WNPs. (**D**) Field-cooled SQUID magnetization curve measured at 4 K for MNPs and WNPs. (**E**) Powder x-ray diffraction spectra of MNPs and WNPs with wüstite (blue) and magnetite (orange) references. a.u., arbitrary units. (**F**) Temperature change in MNP and WNP solutions (4 mg/ml) in response to AMF (H_0 = 15 kA/m and f = 515 kHz). Blue rectangle denotes AMF exposure. Inset shows measured SLP values for MNPs and WNPs under these AMF conditions.

in the presence of MNPs within their growth media (fig. S2). TRPV1 and chromogranin A [CgA, a marker for chromaffin cells of the medulla (*26*)] expression was identified in the cell culture (Fig. 3, C and D). The functional expression of TRPV1 in these cells was further corroborated via Ca^{2+} imaging using a fluorescent indicator Fluo-4. The addition of a TRPV1 agonist CAP stabilized with dimethyl sulfoxide (DMSO) to the cell medium (10 μM final concentration) led to Ca^{2+} influx as marked by an increase in Fluo-4 fluorescence in 60% of the examined cells (n = 140; Fig. 3, E to G). This response was diminished upon addition of a TRPV1 antagonist capsazepine (CZP) (5 μM) (*27*) and was not observed in cultures exposed to DMSO (0.1%) alone (fig. S2).

Magnetothermal adrenal actuation with an externally applied AMF (15 kA/m, 515 kHz) generated in a custom coil driven by a resonant circuit (*28*) was observed in 50% of the examined cells (n = 140) in the presence of MNP solutions (5 mg/ml) (Fig. 3, H to J, and fig. S2). This response was not observed when CZP (5 μM) was added to the cell media before stimulation. The presence of WNPs instead of MNPs resulted in responses from less than 5% of the examined adrenal cells (n = 140; Fig. 3, K to M, and fig. S2) consistent with the negligible heating observed in WNP solutions (Fig. 3M). Together, these experiments suggest that heat-dissipating MNPs are necessary and sufficient to enable remote AMF-mediated actuation of Ca^{2+} influx through TRPV1 channels in adrenal cells.

Remote control of adrenal hormone release

Given the endogenous expression of TRPV1 in the medulla and ZF, we next tested the ability of external AMF stimuli to drive Ca^{2+}-dependent release of epinephrine from the medulla and corticosterone release from the ZF in genetically intact Long-Evans rats in the presence of heat-dissipating MNPs. The secretion of epinephrine and corticosterone results in a rapid increase in the concentration of these hormones in the blood (*16*); hence, we hypothesized that these changes would be detectable in blood serum immediately following magnetothermal stimulation.

To determine the required AMF stimulation parameters, the number of injection sites, and the MNP concentration necessary to trigger TRPV1 channels and the subsequent Ca^{2+} influx into the medulla and ZF cells, while avoiding excessive heating of the adrenal tissue, we developed a finite element model (FEM) of heat distribution within the glands (text S1, table S1, and fig. S3). In addition to the passive heat diffusion from the MNP injection sources, our model accounted for blood perfusion through the gland and a layer of adipose tissue, which acts as thermal insulation. According to the model, two to three small-volume injections as compared to a single combined volume injection offered greater uniformity in heat distribution, allowing for larger stimulation volumes, and reduced tissue exposure to elevated temperatures (Fig. 4A). It was further revealed that in the presence of MNPs at a concentration of 40 mg/ml, 40-s AMF stimulus (15 kA/m, 515 kHz) should be sufficient to reach the TRPV1 threshold temperature (42° ± 1°C; fig. S3) (*29*).

We then developed a surgical procedure to directly inject iron oxide NPs into the rat adrenal glands (Fig. 4B and fig. S4). A total volume of 3 μl per adrenal gland of magnetic MNPs or nonmagnetic WNPs was injected into the appropriate locations within the stabilized organ. One week following the surgery, the rats exhibited normal locomotion indistinguishable from naïve animals (Fig. 4, C to E). Examination of the adrenal glands 6 months following the injection surgeries revealed that NPs persist within the adrenal tissue, causing no notable damage (fig. S5) also observed by hematoxylin and eosin (H&E) staining (Fig. 4F), consistent with the biochemical inertness of iron oxides (*30*). In the postmortem analysis of the adrenal tissue injected with NPs, we found that 80% of the rats harbored injection sites in the adrenal medulla, 90% had injection sites in the ZF and zona reticularis, and only 25% had injection sites in the zona glomerulosa (n = 12; Fig. 5, A and B, text S2, and fig. S6).

To deliver AMF conditions sufficient to drive hysteretic heat dissipation in MNPs injected in adrenal glands, we used a custom apparatus (*28*), capable of producing AMFs with amplitudes up to H = 13.5 ± 1.5 kA/m at a frequency f = 557 kHz (SLP = 620 ± 190 W/g) across a volume of ~200 cm^3, which accommodates an adult Long-Evans rat (Fig. 5, C and D, and fig. S7). The apparatus uses a resonant tank circuit consisting of a capacitor and a parallel water-cooled copper pipe solenoid, which generates the AMFs. To corroborate the

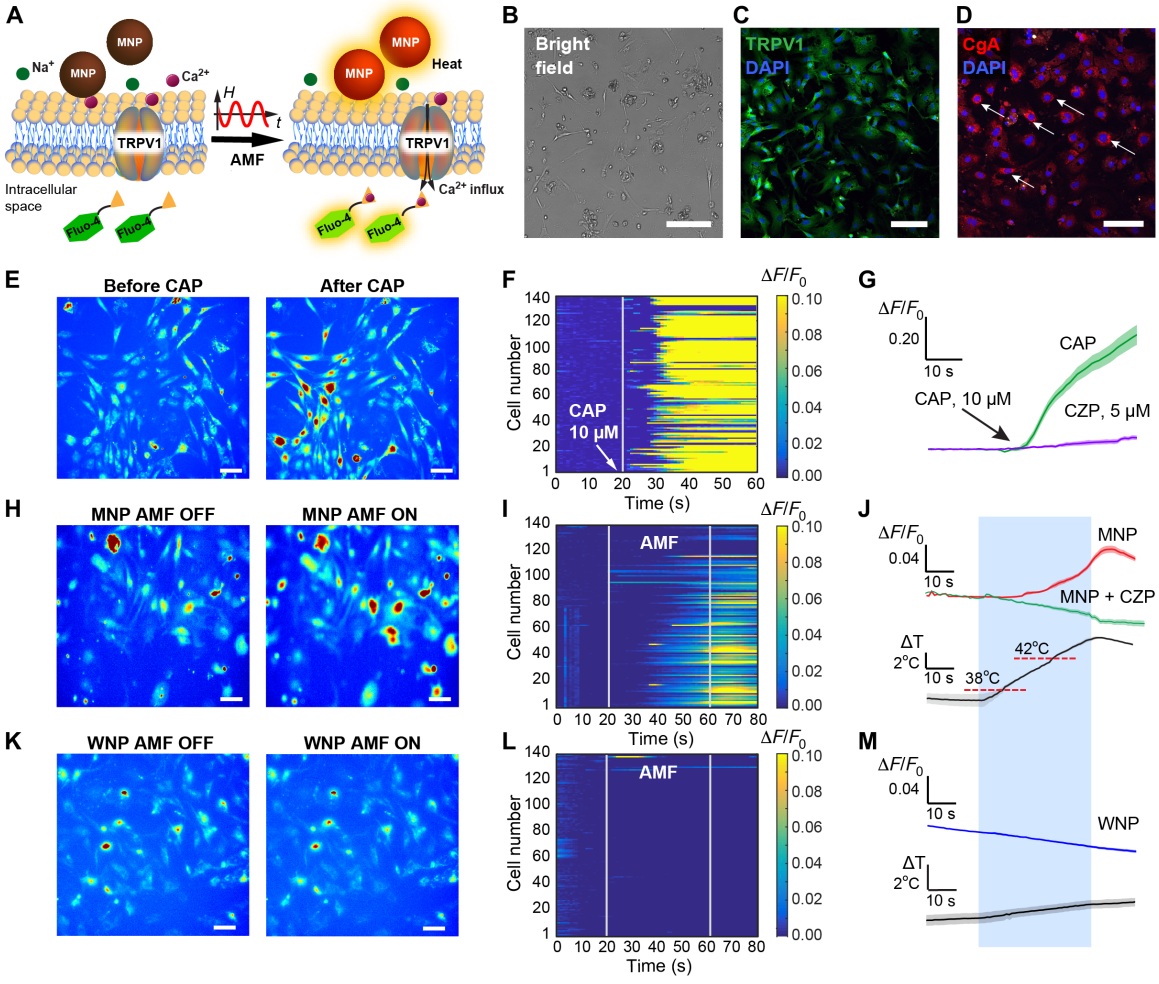

Fig. 3. Magnetothermal stimulation of adrenal cells in vitro. (**A**) Magnetothermal triggering of TRPV1 recorded as a Ca^{2+}-dependent increase in Fluo-4 fluorescence. (**B**) A bright-field micrograph of a primary mixed adrenal cell culture. Scale bar, 50 μm. (**C** and **D**) Expression of TRPV1 (C) (green) and CgA (D) (red) in adrenal cell culture. The nuclear stain DAPI is shown in blue. Scale bars, 100 μm. (**E** to **M**) Ca^{2+} influx in a mixed adrenal cell culture in response to 10 μM CAP (E to G), AMF in the presence of MNPs (H to J), or AMF in the presence of WNPs (K to M). (E, H, and K) Fluo-4 fluorescence images of the mixed adrenal culture before and after CAP (E) or AMF (H and K). Scale bars, 20 μm. (F, I, and L) Normalized Fluo-4 fluorescence intensity for 140 cells versus time. AMF conditions: H_0 = 15 kA/m and f = 515 kHz; duration, 40 s. (G, J, and M) Average fluorescence change ΔF normalized to the average fluorescence F_0 during first 20 s ($\Delta F/F_0$) of recording for cells exposed to CAP with and without CZP (G), cells responding to AMF stimulation in the presence of MNPs without and with CZP (J), and cells responding to AMF in the presence of WNPs (M). Solid line, mean; shaded area, SEM. Blue rectangle denotes AMF exposure.

utility of the AMF stimulation conditions for magnetothermal triggering of adrenal Ca^{2+}, we directly examined hysteretic heating of MNPs driven with our apparatus. An adrenal gland extracted from a rat was injected in two locations with 1 μl of MNPs (40 mg/ml) and placed within the coil. Consistent with our model, a temperature increase of ~5°C was recorded by an infrared camera on the surface of the gland (fig. S7).

The efficacy of magnetothermal adrenal stimulation was first examined by immunoanalysis of expression of an immediate early gene c-*fos*, a marker of activity in electroactive cells, including those in the adrenal gland (Fig. 5, E to G, and fig. S8) (*31*, *32*). One week following the MNP (or WNP) injection surgeries, rats were exposed to 40 s of AMF stimulation (13.5 ± 1.5 kA/m, 557 kHz). We found that 33 ± 4% of adrenal cells in the vicinity of MNP injections expressed c-*fos* following AMF stimulation. In contrast, only 19 ± 3% of cells expressed the biomarker in the vicinity of nonmagnetic and nonheating WNPs ($P < 0.01$, two-sided Student's t test; Fig. 5G). Repeated magnetothermal stimulation of rats injected with MNPs over a period of up to 2 months revealed minimal damage to the gland tissue. Furthermore, the cells in the vicinity of the MNP injections remained responsive to the magnetothermal stimuli (fig. S8).

The release of epinephrine and corticosterone in response to magnetothermal stimulation of adrenal cells was then evaluated in anesthetized rats injected with MNPs or with nonmagnetic WNPs by collecting blood samples (400 μl) at four time points: (i) immediately before AMF exposure, (ii) ≤10 s following 40 s of AMF, (iii) 1 min, and (iv) 4 min following exposure to AMF (Fig. 6A). Blood collection was performed via a chronically implanted jugular vein catheter, and hormone levels in the blood serum were quantified using an enzyme-linked immunosorbent assay (ELISA) and compared to the baseline concentrations. Consistent with the Ca^{2+} influx observed in vitro, up-regulation of c-*fos* in adrenal cells in vivo, and the

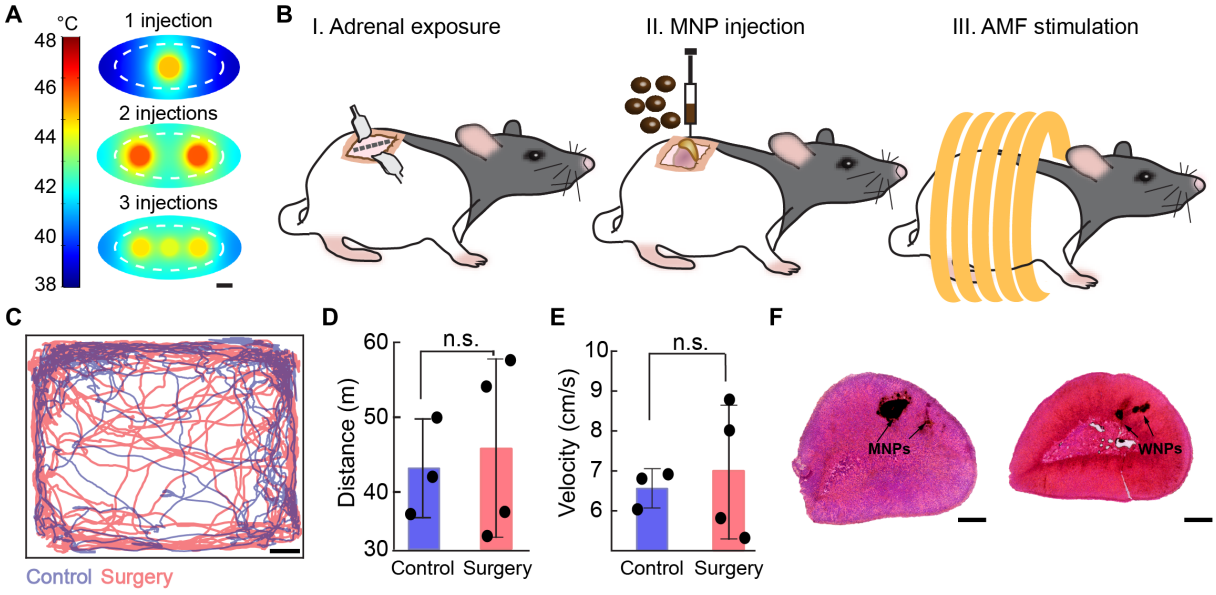

Fig. 4. MNP delivery into adrenal gland. (**A**) FEM of heat distribution within an adrenal gland injected with MNPs (40 mg/ml) in one (1 μl), two (0.8 μl each), or three (0.5 μl each) locations and exposed to AMF for 40 s. The adrenal gland (white dashed line) is surrounded by a layer of adipose tissue. Scale bar, 1 mm. (**B**) Surgical procedure for direct injection of MNPs into the rat adrenal glands 1 week before AMF stimulation. (**C**) Example of tracked positions inside the open field for a rat that underwent an adrenal injection surgery and a control naïve rat. Scale bar, 5 cm. (**D** and **E**) Total distance (means ± std.) traveled by the rats (D) and the average velocity (means ± std.) in the open field during the 10-min test. Control rats ($n = 3$, blue) and postsurgery rats (red, $n = 4$). No significant difference was observed between the two groups (two-sided Student's t test). n.s., not significant. (**F**) H&E staining of rat adrenal glands injected with MNPs and WNPs and extracted 1 to 2 months following surgery. Black arrows indicate MNP and WNP locations. Scale bars, 500 μm.

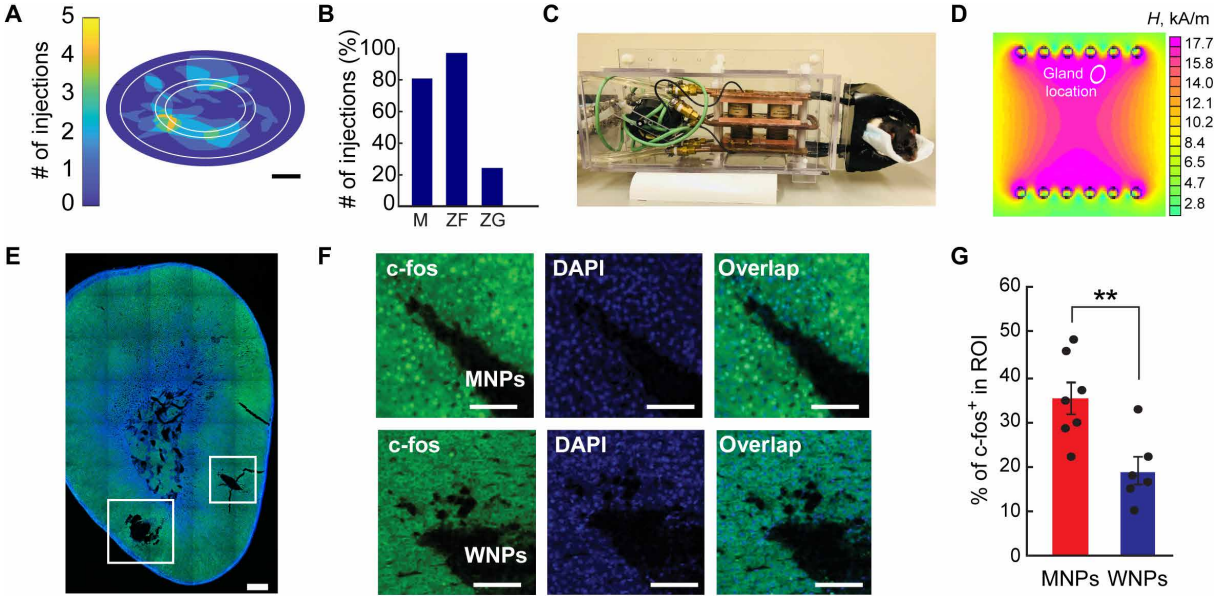

Fig. 5. Magnetothermal stimulation of the adrenal gland in vivo. (**A**) Distribution of NP locations and coverage areas in rats injected in one to three locations ($n = 12$). Scale bar, 1 mm. (**B**) Percent of injection sites out of total examined location sites over 12 examined adrenal gland slices with one to three injection sites in each. (**C**) A photograph of an anesthetized rat in the whole-body AMF stimulation apparatus. (**D**) A Finite Element method magnetic (FEMM) stimulation of anticipated AMF amplitude within the coil under the chosen driving parameters. A white oval indicates an approximate location of the adrenal glands during the stimulation experiments. The AMF amplitude values are consistent with those necessary to achieve high SLPs. (**E** and **F**) Confocal images of the c-fos immunofluorescence in the adrenal gland following AMF stimulation. (**E**) A mosaic of an entire slice of an adrenal gland injected with MNPs in two locations (white squares). Scale bar, 300 μm. (**F**) Confocal images in the presence of MNPs (top) or WNPs (bottom). Scale bars, 100 μm. (**G**) Percentage of the *c-fos*–expressing cells in the region of interest (ROI) following AMF stimulation in rats injected with MNPs or WNPs. Error bars represent means ± SEM (number of injection sites per group: MNPs, $n = 7$ and WNPs, $n = 5$. Two-sided Student's t test with threshold $^{**}P < 0.01$, $P = 0.006$). Photo credit: Dekel Rosenfeld, Massachusetts Institute of Technology.

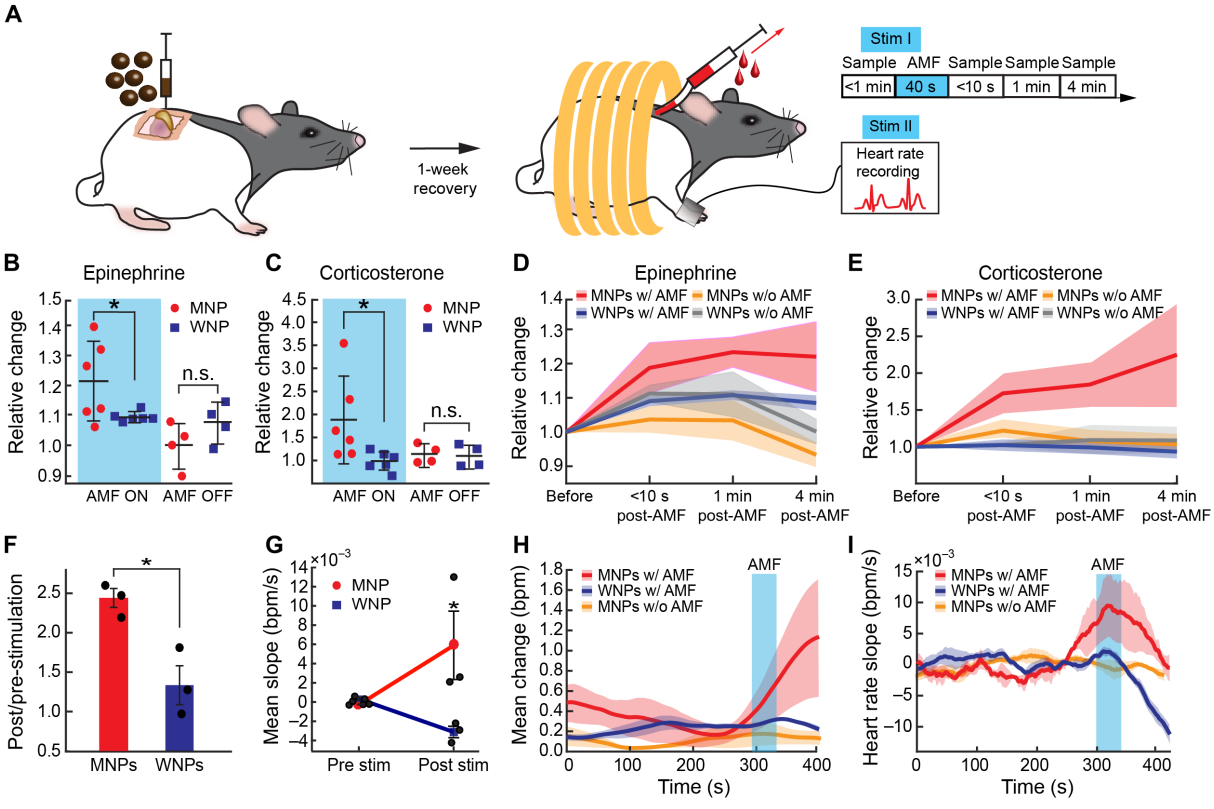

Fig. 6. Magnetothermal regulation of adrenal hormones in vivo. (**A**) Timeline for injection of MNPs into the adrenal glands and blood sampling through a jugular vein catheter. Heart rate recordings are performed on a separate day. (**B** and **C**) Normalized relative change in epinephrine (B) and corticosterone (C) concentrations averaged across the three time points following AMF stimulation as compared to the baseline level for each rat before AMF [*P < 0.05, one-way analysis of variance (ANOVA) followed by two-sided Student's t test with threshold; epinephrine, P = 0.029; corticosterone, P = 0.038]. (**D** and **E**) Normalized relative change in epinephrine and corticosterone across four time points. Solid lines and shaded areas represent means and SEM, respectively [(B) to (E): n = 6 in WNP/MNP with AMF and n = 4 WNP/MNP without AMF]. (**F**) Ratio of the poststimulation (post) to prestimulation (pre) heart rates (*P < 0.05, two-sided Student's t test with threshold, means ± SEM, n = 3, P = 0.018). (**G**) Average of relative heart rate slope [beats per minute per second (bpm/s)] from pre-stimulation baseline (pre stim) to post stimulation (post stim) values (*P < 0.05, one-sided Student's t test with threshold, means ± SEM, n = 3, P = 0.033). (**H**) Mean change in heart rate measured before, during, and after exposure to AMF. (**I**) Heart rate slope (bpm/s) as measured before, during, and after exposure to AMF. (H and I) Solid lines and shaded areas represent means ± SEM, n = 3 per group. Blue rectangles denote AMF exposure.

distribution of injection sites across the medulla and ZF, AMF stimulus evoked an 80 ± 4% increase in corticosterone and a 21 ± 5% increase in epinephrine concentrations as compared to the baseline levels in rats injected with MNPs but not in those injected with WNPs (Fig. 6, B and C). An examination of temporal dynamics of the hormone release across the four time points revealed that epinephrine levels appeared to stabilize within 1 min following AMF stimulation (Fig. 6D). In contrast, corticosterone levels continued to increase even 4 min after the AMF stimulus was turned off, which is consistent with the physiological release profiles of this hormone (Fig. 6E) (*33*). No significant changes in adrenal hormone levels were observed in control subjects injected with MNPs and placed within the apparatus but not exposed to AMF and those injected with WNPs and exposed or not exposed to AMF (Fig. 6, B to E).

Epinephrine release into the circulatory system results in an increased heart rate (*16*), which we have corroborated by intraperitoneal epinephrine administration to a naïve rat (fig. S9). Therefore, we hypothesized that epinephrine release from the adrenal medulla in response to magnetothermal stimulation will be accompanied by an increase in heart rate. To test this, we repeated the stimulation protocol used for blood analysis (Fig. 6A) and monitored the heart rate throughout the experiment. As anticipated, magnetothermal stimulation led to an increase in the heart rate and its slope in rats injected with MNPs in the adrenal medulla (Fig. 6, F and G, text S3, and fig. S9). No significant increase in the heart rate or its slope was observed in the absence of AMF or in rats injected with nonmagnetic WNPs (Fig. 6, F to I).

DISCUSSION

We designed a transgene-free magnetothermal stimulation approach for temporally precise remote control of hormone secretion from the adrenal gland. The technique relies on hysteretic heating of MNPs in response to weak, externally applied, rapidly AMFs to trigger endogenously expressed heat-sensitive TRPV1 channels and Ca^{2+} influx into the cells in the adrenal medulla and cortex. Our results demonstrate that MNPs persist within the tissue for up to 6 months and allow for chronic stimulation of the adrenal gland over days and weeks with no observable damage to the tissue integrity or cell function.

By using MNPs as transducers of weak magnetic field, magnetothermal stimulation effectively decouples penetration depth from the resolution and reduces the impact on the surrounding untargeted tissue. Furthermore, advances in surface chemistry and synthetic biology can enable both genetic and nongenetic targeting of specific

cells by using antibodies against membrane proteins or by relying on transgenes of engineered targeting moieties (*10*). In addition, a multiplexing approach can be adopted to individually control the release of specific hormones from different adrenal layers. Magnetothermal multiplexing allows us to separately control heat dissipation from at least two populations of MNPs with differing coercivities by tuning the AMF conditions (*34*). For instance, a multiplexed strategy could in the future be applied to independent control of epinephrine and corticosterone from the adrenal medulla and ZF, respectively. Furthermore, future translational applications will likely require a closed-loop system to continuously monitor hormone levels in the blood to achieve or maintain the desired extent of hormone release.

To account for potential effects associated with the presence of iron-containing NPs in the tissue, we relied on WNPs that share the elemental composition with MNPs yet have a distinct crystal structure with markedly different magnetic properties. As no effects on cell signaling were identified in response to AMF in the presence of the WNPs, we believe that these particles not only serve as controls for magnetothermal modulation but also offer insights into the importance of structure rather than atomic composition alone in the design of transducers of magnetic fields.

The number of the NPs at the injection site could, in principle, decrease via either diffusion or endocytosis and digestion with lysosomes. The efficacy of the magnetothermal stimulation was demonstrated even 2 months after the MNP injection, suggesting a nonsignificant decrease in the concentration of the MNPs at the injection site and a nonsignificant change in their magnetic properties. The latter was also verified by observing only negligible changes in MNP saturation magnetization following incubation in physiological conditions for 8 days (fig. S2).

Potential mechanisms underlying magnetothermal response include direct triggering of Ca^{2+} permeable heat-sensitive ion channels (*29*) and thermal effects on the membrane capacitance (*35*). Here, we demonstrate the broad distribution of TRPV1 expression in the adrenal gland and show that magnetothermal stimulus can be rendered ineffective in the presence of the TRPV1 blocker CZP. Therefore, we suggest TRPV1 triggering as a key mechanism mediating magnetothermal control over adrenal function. This hypothesis can be further refined in the future by examining the adrenal expression profiles of other thermally sensitive members from the TRP family (*36*, *37*).

Relying on the endogenous TRPV1 response implies that other hormones from other substructures of the adrenal gland could, in principle, be released, for example, aldosterone from the zona glomerulosa. To account for such nonspecific hormone release, further investigation of TRPV1 expression in the zona glomerulosa is needed and investigation of the potential involvement of Ca^{2+} influx in aldosterone release. Improved MNP targeting, especially in larger organisms, could likely overcome these possible side effects that are anticipated to be more pronounced in small rodents. A possibility of mechanical effects from the interaction of the AMF and the MNPs can be ruled out as the energies and forces necessary to excite mechanosensitive ion channels exceed those that can be generated for the MNP dimensions and AMF conditions used in our study by orders of magnitude (text S4).

TRPV1 (and other heat-sensitive TRP channels) were shown to be expressed in other organs deep within the body such as the peripheral nerves, gastrointestinal tract (*38*), pancreas, (*39*) and heart (*40*), suggesting potential applications for magnetothermal deep organ stimulation as means to study organ function and pave the way to development of bioelectronic medicines.

MATERIALS AND METHODS

All solvents and reagents were purchased from Sigma-Aldrich unless otherwise mentioned.

NP synthesis

Iron oxide MNPs were synthesized according to Chen *et al.* (*23*). Briefly, iron-oleate complex was synthesized in a three-neck flask by heating to reflux (60°C) 92 mmol of sodium oleate (95%, TCI America) and 30 mmol of $FeCl_3{\cdot}6H_20$ (99%, Acros) in a solvent mixture of 200 ml of hexane, 100 ml of ethanol, and 100 ml of double distilled water for 1 hour under N_2. The mixture was heated to 110°C and dried overnight on a hotplate.

For preparing MNPs, the iron-oleate mixture was degassed at 90°C for 1 hour with a combination of 2:1 (volume ratio) of 1-octadecence (90%, 10 ml) and dibenzyl ether (98%, 5 ml). Then, the mixture was heated to 200°C under N_2. For preparing WNPs, the same procedure was performed but with 20 ml of 1-octadecene as solvent. Following this step, all mixtures were heated to 200°C under N_2 and then to reflux at ~325°C for 30 min. After pelleting and washing, all NPs were redispersed in 5 ml of chloroform.

Phase transfer of NPs

PEG was grafted with PMAO through mixing in ratio of 3:1 (respectively) in 30 ml of chloroform and in the presence of 50 μl of concentrated sulfuric acid, refluxing overnight at 61°C. For labeling MNPs with Rhodamine, PMAO was reacted with Rhodamine123 followed by reaction with PEG (5 kDa) resulting in PMAO-Rh-PEG polymer.

After washes of the sulfuric acid using a combination of hexane and ethanol, the polymeric blend was dried in a desiccator overnight. For NP coating, PEG-PMAO powder was resuspended in chloroform (10 mg/ml) and sonicated with NP ferrofluid (10 mg/ml) for 1 hour. After solvent removal, NPs were suspended in tris-borate EDTA buffer (1×) and washed three times with double distilled water. NPs were stored in water until used.

Characterization of NPs

The NP concentration was measured using inductively coupled plasma optical emission spectrometry (ICP-OES) (Agilent 5100 DVD), and their saturation magnetization was calculated on the basis of their concentration and saturation moment measured using MPMS3 superconducting quantum interference device (SQUID)–vibrating sample magnetometry (VSM) (Quantum Design Inc.) at 4 and 260 K for both MNPs and WNPs. For estimating the SLP of the NPs based on the dynamic hysteresis model (*34*), we used a similar method as described in the previous work of our group. Briefly, NPs (with a concentration of 4 mg/ml, $n = 3$) were placed in small glass vial together with an optical fiber temperature probe (Omega HHTFO-101). The sample was placed in a 7.5-mm gap of a toroidal ferromagnetic core that is driven by a custom-built series resonant circuit. A voltage signal was generated using a function generator amplified by a 200-W amplifier (1020L, Electronics & Innovation), generating AMF with frequency $f = 515$ kHz and amplitude $H_0 = 15$ kA/m. The field amplitude was measured using an inductive pick-up coil of known geometry and an oscilloscope.

To examine possible changes in the magnetic properties of the MNPs in physiological conditions, PEG-PMAO–coated MNPs were incubated for 8 days in physiological conditions in phosphate-buffered saline (PBS) in the incubator (37°C). The new concentration of the MNPs was measured using ICP-OES, and magnetization curves were generated using VSM for MNPs before and after incubation.

Immunohistochemistry and imaging of adrenal slices

All animal procedures were approved by the Massachusetts Institute of Technology (MIT) Committee on Animal Care. For c-fos expression analysis, rats were anesthetized at least 1 week after MNP injection and were stimulated with AMF for 40 s. After stimulation, rats were kept anesthetized for 60 min to allow for c-fos expression. For all immunostaining, rats received intraperitoneal injection with Fatal-Plus Solution (100 mg/kg in PBS) and were transcardially perfused with 4% paraformaldehyde (PFA; Electron Microscopy Sciences) in PBS. For examination of long-term effects and efficiency of the magnetothermal stimulation, a group of rats injected with MNPs were exposed to repeated stimulations over a period of up to 2 months, and on the last stimulation, rats were perfused as described above.

Following perfusion, the adrenal gland was extracted from the rat and fixed in 4% PFA overnight. After three washes with PBS, all adrenal glands were embedded in 5% agarose and sliced into 40-μm slices using a vibrating blade microtome (Leica VT1000S). Slices were then permeabilized with 0.3% (v/v) Triton X-100 and blocked with 5% goat/donkey serum in PBS for 30 min. Slices were incubated overnight at 4°C in a solution of primary antibodies and 5% goat/donkey serum (depending on secondary) in PBS. After three washes of the slices with PBS, incubation with secondary antibody in PBS was performed for 3 hours and with DAPI (4′6-diamidino-2-phenylindole) (1:50,000) for another 20 min and washed three times with PBS. Fluoromount-G (SouthernBiotech) was used for mounting slices onto glass microscope slides. A laser scanning confocal microscope (FluoView FV1000, Olympus) was used for imaging with 4×, 20×, and 60× objectives. Mosaic images of the entire slices were generated by the FV1000 software (Olympus). H&E was performed on the adrenal slices using the manufacturer's standard protocol, and after mounting, slices were imaged using EVOS imaging system.

The following antibodies were used

Target	Primary antibody	Secondary antibody
c-fos	Rabbit anti–c-fos (sc-253, Santa Cruz Biotechnology)	488 goat anti-rabbit (Invitrogen)
TRPV1	Rabbit anti-TRPV1 (AB5889, Millipore)	488 donkey anti-rabbit (Invitrogen)
TRPV1	Guinea pig (Gp) anti-TRPV1 (AB5566, Millipore)	Cy3, donkey anti-Gp (Jackson ImmunoResearch Laboratories)
SYN	Mouse anti-SYN (MAB329, Millipore)	568, donkey anti-mouse (Invitrogen)
CGRP	Rabbit anti-CGRP (AB15360, Millipore)	488, donkey anti-rabbit (Invitrogen)

Image analysis

Image analysis for the quantification of immunostaining was performed using custom algorithms written in MATLAB (MathWorks) and available upon request. For c-*fos* expression, the area of NPs (WNPs or MNPs) injection was identified in the entire mosaic of the slice and marked using the function "roipoly." The region of interest (ROI) was then defined as a square around the injection area with twice the area of the NP-covered area. Positive c-fos cells were counted if they overlapped with DAPI, and the percentage of c-fos–positive cells of all cells in the ROI was calculated.

For protein expression analysis of TRPV1, SYN, a mask was created around each cell nucleus identifying positive staining in the vicinity of each cell (twice the area of the cell nucleus). For colocalization, only areas that had an overlap of both channels were counted positive. The percentage of positive cells was calculated out of the total examined cells in each image. Each protein was averaged in at least three biological replicates ($n \geq 3$ rats).

Adrenal gland cell culture

Krebs-Ringer buffer solution (KRBG): 115 mM NaCl (MACRON), 1.9 mM KCl, 1.5 mM $CaCl_2$, 1.9 mM KH_2PO_4, 0.2% glucose, 0.62 mM GlutaMAX (Life Technologies), 25 mM $NaHCO_3$, 1 mM $MgSO_4{\cdot}7H_2O$ (Fisher Chemicals), 0.1% bovine serum albumin, 2% minimum essential medium (MEM) amino acid solution (Gibco), and 1% MEM nonessential amino acid solution (Gibco). Cell medium: Opti-MEM (Gibco) medium supplemented with 5% fetal bovine serum and 1% penicillin-streptomycin solution (Lonza).

Five-millimeter-round glass coverslips were acid etched with 37% HCl solution (Sigma-Aldrich, St. Louis, MO) and then washed and stored in ethanol. Before cell seeding, coverslips were dried thoroughly and placed in a 24-well tissue culture plate with three coverslips in each well. Coverslips were coated with a 1:30 dilution of Matrigel (BD Biosciences, San Jose, CA) in cell medium and kept in 37°C overnight before cell seeding. Adrenal glands were extracted from male Long-Evans rats and immediately placed in KRBG solution on ice, as adopted from previously published protocols. The fat layer was removed gently from the gland, and the gland was dissociated by incubating in collagenase solution (4 mg/ml; Sigma, St. Louis, MO) with deoxyribonuclease (0.04 mg/ml) for 1 hour in 37°C (4 glands/3 ml). Following incubation, the glands were mechanically disrupted by gentle aspiration with a sterile 5-ml pipette, and excessive parts of the tissue were filtered using a 40-μm nylon mesh cell strainer (Corning). Cells were washed twice with cold KRBG solution and then incubated in cell medium for 30 min in 37°C before seeding. Cells were seeded on the coated coverslips dividing cells from one gland over three wells.

Immunostaining analysis was performed on cells seeded on the coverslips and fixed for 20 min in 4% PFA. After three washes with PBS, cells were permeabilized with 0.3% (v/v) Triton X-100 and blocked with 5% goat/donkey serum in PBS for 30 min. Cells were incubated for 2 hours at room temperature in a solution of primary antibodies and 5% goat/donkey serum (depending on secondary) in PBS. After three washes of the cells with PBS, incubation with secondary antibody in PBS was performed for 2 hours and with DAPI (1:50,000) for another 15 min and washed three times with PBS. Fluoromount-G (SouthernBiotech) was used for mounting the coverslips onto glass microscope slides.

The following antibodies were used

Target	Primary antibody	Secondary antibody
TRPV1	Rabbit anti-TRPV1 (AB5889, Millipore)	488 donkey anti-rabbit (Invitrogen)
CgA	Mouse anti-CgA (MAB5268, Millipore)	568 donkey anti-mouse (Invitrogen)

Biocompatibility and viability tests

Following cell culture, a Live/Dead Viability/Cytotoxicity assay (Invitrogen) was used to examine the percentage of live cells (via calcein AM) and dead cells (via ethidium homodimer-1) in the culture, and the different cell populations in the mixed adrenal culture were imaged using a confocal microscope (Olympus).

To examine the biocompatibility of MNPs with adrenal cell culture, the alamarBlue metabolic assay (Thermo Fisher Scientific) was used. On day 0 (baseline), cells were incubated with alamarBlue solution (1:10 in cell medium) for 4 hours, followed by fluorescent intensity reading using a plate reader with 545-nm excitation and 590-nm emission. MNP solution with a concentration of 0.5 mg/ml was added to cell medium, and cells were incubated with the ferrofluid solution for 1, 2, 4, and 7 days (n = 3 wells). On each day, the alamarBlue test was repeated to examine cell viability and proliferation.

NP uptake by adrenal cells

To examine possible internalization of MNPs into adrenal cells, MNPs labeled with Rhodamine (Rh-MNP) were incubated for 24 hours with adrenal cells. After 24 hours, cells were washed with cell medium. Adrenal cells were labeled with Fluo-4, and the cells were visualized under confocal microscope with ×20 and ×60 magnifications to examine whether labeled MNPs can be traced inside the cells. Quantification of cell uptake of MNPs was performed in ImageJ. Cells with internalized MNPs were identified and counted manually. In addition, cells seeded on 5-mm coverslips coated with Matrigel were incubated in a 96-well plate with the labeled Rh-MNP for 24 hours. Following one wash with cell medium, the fluorescence intensity was measured in a plate reader subtracting the blank measurement of medium only. Two control groups were examined: cells incubated for 24 hours with nonlabeled MNPs and coverslips coated with Matrigel that were incubated for 24 hours with labeled Rh-MNP.

Imaging of adrenal cell cultures

Magnetothermal stimulation effects on adrenal cell culture were assessed through calcium imaging on adrenal cell culture using the calcium dye indicator Fluo-4 (Invitrogen). For all experiments, 1 mM of Fluo-4 (Invitrogen) in DMSO (99.9%) was diluted 1000× in the cell medium and incubated with the cells for 45 min in 37°C. Cells were then transferred to the preheated Tyrode's solution (37°C) for fluorescent imaging using an inverted fluorescence microscope (Olympus).

For assessing the effect of CAP (TCI America) on calcium influx to the cells through the TRPV1 ion channel, 0.1 M CAP in DMSO was administered to the cells rapidly, after a 20-s baseline imaging, and the imaging was continued for another 60 s. The final concentration of CAP incubated with the cells was 10 μM (total 0.1% DMSO). The specificity to the CAP and TRPV1 ion channel response was assessed using CZP (no. 0464, Tocris), a TRPV1 antagonist. Following the incubation with Fluo-4 and while cells were in Tyrode's solution, cells were incubated with 5 μM CZP for 20 min and then imaged with CAP, similar to the method described above. A control experiment in which cells were incubated with DMSO instead of CAP was conducted similarly by replacing the CAP or the CZP with DMSO in the same volume of DMSO that was used in the experiments. The gapped coil described for calorimetry measurement was used while placed on the inverted microscope, allowing imaging and AMF stimulation in the gap of the coil with the cells seeded on the 5-mm coverslips located in the gap.

For magnetothermal stimulation simultaneously with calcium imaging, the resonant circuit coil, described above for calorimetry, was used to apply magnetic field on 5-mm coverslips seeded with mixed adrenal cells following the incubation with Fluo-4. The gap of the coil with the sample was located above the microscope objective for imaging. Cells were placed into the NPs solution (5 mg/ml in Tyrode's solution) before the start of the stimulation, and after 20 s of baseline imaging, 40 s of stimulation with AMF was applied. MNP or WNP solutions in Tyrode were preheated to 35° to 37°C before the start of the experiment. The temperature of the ferrofluid was continuously monitored using a temperature probe inside the solution.

Analysis of calcium imaging data

Using the Olympus CellSens software, .vsi videos were collected for all the calcium imaging. All experiments were imaged for 60 to 80 s. The .vsi files were opened using the Bio-Formats package in ImageJ and after setting a threshold, cells were manually marked in the movie, and the average grayscale values were generated. Further analysis was conducted using a custom script in MATLAB that converted the measured fluorescent intensity values to $\Delta F/F_0$ traces. F_0 was the average fluorescence intensity for each examined cell for the first 20 s (the baseline measurement) and was used to compute $\Delta F = F - F_0$ for each frame measured. In total, we examined 140 cells in each examined condition and control group. A heat map was generated in MATLAB for all 140 examined cells, and the average of the responding cells was calculated. Cells were counted as responders if their $\Delta F/F_0$ ever exceeded 10 times the SD of the signal during the period before the start of stimulation.

Surgical procedure for NP injections into the rat adrenal glands

All animal procedures were approved by the MIT Committee on Animal Care. As commonly used in neuroscience studies of posttraumatic stress and depression, we used Long-Evans rats for all magnetothermal stimulations. All surgical procedures and stimulations were performed under inhalable isoflurane anesthesia, 1 to 3.5%, in oxygen. We started with an exposure of an adrenal gland through an incision through the skin and muscle tissue above the kidney on the abdomen of the rat. The gland was then identified and stabilized using a pair of sterile Q-tips to avoid movement during NP solution injection via a microsyringe held in a stereotactic manipulator into the appropriate location in the gland. NP solution was injected in one to three locations inside the gland with a volume of 0.5 to 1 μl and injection rate of 0.1 μl/min. At the end of the injection, the needle was kept inside the gland for another 10 min to prevent leakage of ferrofluid solution. The muscle and the skin are then sutured, and the rats recover for at least 1 week before AMF stimulation.

Open-field test of locomotion

One week after surgery, a standard open-field test was performed using a custom chamber (made of opaque polycarbonate) with dimensions of 60 cm by 60 cm by 40 cm. Rats were brought to the room in their home cage 2 hours before the start of the experiment. Rats were placed in the center of the open field for 10 min while continuously imaged with a camera suspended above the chamber. Tracking of rat position was performed using custom Python code. The speed and total distance were calculated from the tracking data.

Magnetothermal stimulation in vivo

One week following the surgical procedure, rats were anesthetized and placed within the in vivo coil for magnetothermal stimulation.

The rat was placed on movable bed placed inside the coil, avoiding any contact of the rat body with the coil itself to prevent heating of the body during stimulation (although the coil system is actively cooled and thus does not heat significantly). The adrenal gland was located in approximately the same location as the phantom extracted adrenal was positioned, resulting in a stable and sufficient field amplitude during the stimulation. The values of field amplitude chosen were matched to the necessary field amplitude to reach an SLP of above 600 W/g as was modeled in the FEM.

Hormone quantification using ELISA assays

Using a jugular vein catheter, blood samples were collected before and after stimulation. Blood was collected into a serum separator tube (Thermo Fisher Scientific) and allowed to clot on ice for 1 hour. Samples were centrifuged for 10 min at 3000*g* at 4°C. Serum was immediately collected and kept in aliquots at −20°C until used.

ELISA was performed using the ELISA kits of MyBioSource (Epinephrine: MBS264776; Corticosterone: MBS761865) according to the manufacturer's protocol. A plate reader was used to read the optical density at the end of the ELISA assay, and values were calculated according to a calibration curve, which was obtained separately for each tested plate.

Heart rate measurements

Heart rate was monitored and recorded during magnetothermal stimulation using a PhysioSuite System (Kent Scientific) and a paw optical sensor. A baseline measurement was conducted, ensuring that there is no influence on the heart rate measurement during the AMF stimulation. To examine the possible effects of hormone release on the rat's heart rate using our systems and measurement techniques, we injected either epinephrine (10 to 20 μg/mg) or the beta-blocker labetalol (0.5 mg/kg) subcutaneously.

SUPPLEMENTARY MATERIALS

Supplementary material for this article is available at http://advances.sciencemag.org/cgi/content/full/6/15/eaaz3734/DC1

View/request a protocol for this paper from *Bio-protocol*.

REFERENCES AND NOTES

1. M. G. Arnett, L. M. Muglia, G. Laryea, L. J. Muglia, Genetic approaches to hypothalamic-pituitary-adrenal axis regulation. *Neuropsychopharmacology* **41**, 245–260 (2015).
2. S. A. Kinlein, C. D. Wilson, I. N. Karatsoreos, Dysregulated hypothalamic–pituitary–adrenal axis function contributes to altered endocrine and neurobehavioral responses to acute stress. *Front. Psychol.* **6**, 31 (2015).
3. B. Hruska, P. K. Cullen, D. L. Delahanty, Pharmacological modulation of acute trauma memories to prevent PTSD: Considerations from a developmental perspective. *Neurobiol. Learn. Mem.* **112**, 122–129 (2014).
4. V. A. Pavlov, K. J. Tracey, The vagus nerve and the inflammatory reflex—Linking immunity and metabolism. *Nat. Rev. Endocrinol.* **8**, 743–754 (2012).
5. V. Pikov, A. Sridhar, H. E. Lara, High-frequency electrical modulation of the superior ovarian nerve as a treatment of polycystic ovary syndrome in the rat. *Front. Physiol.* **9**, 459 (2018).
6. V. Walsh, A. Cowey, Transcranial magnetic stimulation and cognitive neuroscience. *Nat. Rev. Neurosci.* **1**, 73–79 (2000).
7. J. O. Szablowski, A. Lee-Gosselin, B. Lue, D. Malounda, M. G. Shapiro, Acoustically targeted chemogenetics for the non-invasive control of neural circuits. *Nat. Biomed. Eng.* **2**, 475–484 (2018).
8. O. Yizhar, L. E. Fenno, T. J. Davidson, M. Mogri, K. Deisseroth, Optogenetics in neural systems. *Neuron* **71**, 9–34 (2011).
9. Q. A. Pankhurst, J. Connolly, S. K. Jones, J. Dobson, Applications of magnetic nanoparticles in biomedicine. *J. Phys. D. Appl. Phys.* **36**, R167 (2003).
10. H. Huang, S. Delikanli, H. Zeng, D. M. Ferkey, A. Pralle, Remote control of ion channels and neurons through magnetic-field heating of nanoparticles. *Nat. Nanotechnol.* **5**, 602–606 (2010).
11. R. Chen, G. Romero, M. G. Christiansen, A. Mohr, P. Anikeeva, Wireless magnetothermal deep brain stimulation. *Science* **347**, 1477–1480 (2015).
12. S. A. Stanley, J. E. Gagner, S. Damanpour, M. Yoshida, J. S. Dordick, J. M. Friedman, Radio-wave heating of iron oxide nanoparticles can regulate plasma glucose in mice. *Science* **336**, 604–608 (2012).
13. S. Schuerle, J. S. Dudani, M. G. Christiansen, P. Anikeeva, S. N. Bhatia, Magnetically actuated protease sensors for in vivo tumor profiling. *Nano Lett.* **16**, 6303–6310 (2016).
14. R. Munshi, S. M. Qadri, Q. Zhang, I. C. Rubio, P. del Pino, A. Pralle, Magnetothermal genetic deep brain stimulation of motor behaviors in awake, freely moving mice. *eLife* **6**, e27069 (2017).
15. Q. Yu, Y. Wang, Y. Yu, Y. Li, S. Zhao, Y. Chen, A. B. Waqar, J. Fan, E. Liu, Expression of TRPV1 in rabbits and consuming hot pepper affects its body weight. *Mol. Biol. Rep.* **39**, 7583–7589 (2012).
16. A. M. de Diego, L. Gandia, A. G. García, A physiological view of the central and peripheral mechanisms that regulate the release of catecholamines at the adrenal medulla. *Acta Physiol.* **192**, 287–301 (2008).
17. T. J. Rosol, J. T. Yarrington, J. Latendresse, C. C. Capen, Adrenal gland: structure, function, and mechanisms of toxicity. *Toxicol. Pathol.* **29**, 41–48 (2001).
18. A. G. García, A. M. García-De-Diego, L. Gandía, R. Borges, J. García-Sancho, Calcium signaling and exocytosis in adrenal chromaffin cells. 86, 1093–1131 (2006).
19. J. J. Enyeart, J. A. Enyeart, Ca^{2+} and K^+ channels of normal human adrenal zona fasciculata cells: Properties and modulation by ACTH and AngII. *J. Gen. Physiol.* **142**, 137–155 (2013).
20. P. N. Surkin, S. L. Gallino, V. Luce, F. Correa, J. Fernandez-Solari, A. De Laurentiis, Pharmacological augmentation of endocannabinoid signaling reduces the neuroendocrine response to stress. *Psychoneuroendocrinology* **87**, 131–140 (2018).
21. B. Wiedenmann, W. W. Franke, Identification and localization of synaptophysin, an integral membrane glycoprotein of Mr 38,000 characteristic of presynaptic vesicles. *Cell* **41**, 1017–1028 (1985).
22. H. Kuramoto, H. Kondo, T. J. C. Fujita, Calcitonin gene-related peptide (CGRP)-like immunoreactivity in scattered chromaffin cells and nerve fibers in the adrenal gland of rats. *Cell Tissue Res.* **247**, 309–315 (1987).
23. R. Chen, M. G. Christiansen, A. Sourakov, A. Mohr, Y. Matsumoto, S. Okada, A. Jasanoff, P. Anikeeva, High-performance ferrite nanoparticles through nonaqueous redox phase tuning. *Nano Lett.* **16**, 1345–1351 (2016).
24. R. Chen, M. G. Christiansen, P. Anikeeva, Maximizing hysteretic losses in magnetic ferrite nanoparticles via model-driven synthesis and materials optimization. *ACS Nano* **7**, 8990–9000 (2013).
25. C. A. McCammon, Magnetic properties of Fe_xO ($x > 0.95$): Variation of Néel temperature. *J. Magn. Magn. Mater.* **104-107**, 1937–1938 (1992).
26. K. B. Helle, M.-H. Metz-Boutigue, M. C. Cerra, M. C. Cerra, T. Angelone, Chromogranins: From discovery to current times. *Pflugers Arch.* **470**, 143–154 (2018).
27. S. Bevan, S. Hothi, G. Hughes, I. F. James, H. P. Rang, K. Shah, C. S. J. Walpole, J. C. Yeats, Capsazepine: A competitive antagonist of the sensory neurone excitant capsaicin. *Br. J. Pharmacol.* **107**, 544–552 (1992).
28. M. G. Christiansen, C. M. Howe, D. C. Bono, D. J. Perreault, P. Anikeeva, Practical methods for generating alternating magnetic fields for biomedical research. *Rev. Sci. Instrum.* **88**, 084301 (2017).
29. M. J. Caterina, M. A. Schumacher, M. Tominaga, T. A. Rosen, J. D. Levine, D. Julius, The capsaicin receptor: A heat-activated ion channel in the pain pathway. *Nature* **389**, 816–824 (1997).
30. M. Marcus, M. Karni, K. Baranes, I. Levy, N. Alon, S. Margel, O. Shefi, Iron oxide nanoparticles for neuronal cell applications: Uptake study and magnetic manipulations. *J. Nanobiotechnology* **14**, 37 (2016).
31. M. Pelto-Huikko, Å. Dagerlind, S. Ceccatelli, T. Hökfelt, The immediate-early genes c-*fos* and c-*jun* are differentially expressed in the rat adrenal gland after capsaicin treatment. *Neurosci. Lett.* **126**, 163–166 (1991).
32. T. C. Wessel, T. H. Joh, Parallel upregulation of catecholamine-synthesizing enzymes in rat brain and adrenal gland: Effects of reserpine and correlation with immediate early gene expression. *Mol. Brain Res.* **15**, 349–360 (1992).
33. R. M. Sapolsky, L. M. Romero, A. U. Munck, How do glucocorticoids influence stress responses? Integrating permissive, suppressive, stimulatory, and preparative actions. *Endocr. Rev.* **21**, 55–89 (2000).
34. M. G. Christiansen, A. W. Senko, R. Chen, G. Romero, P. Anikeeva, Magnetically multiplexed heating of single domain nanoparticles. *Appl. Phys. Lett.* **104**, 213103 (2014).
35. M. G. Shapiro, K. Homma, S. Villarreal, C.-P. Richter, F. Bezanilla, Infrared light excites cells by changing their electrical capacitance. *Nat. Commun.* **3**, 736 (2012).

36. K. Talavera, K. Yasumatsu, T. Voets, G. Droogmans, N. Shigemura, Y. Ninomiya, R. F. Margolskee, B. Nilius, Heat activation of TRPM5 underlies thermal sensitivity of sweet taste. *Nature* **438**, 1022–1025 (2005).
37. T. Voets, K. Talavera, G. Owsianik, B. Nilius, Sensing with TRP channels. *Nat. Chem. Biol.* **1**, 85–92 (2005).
38. A. Akbar, Y. Yiangou, P. Facer, J. R. Walters, P. Anand, S. Ghosh, Increased capsaicin receptor TRPV1-expressing sensory fibres in irritable bowel syndrome and their correlation with abdominal pain. *Gut* **57**, 923–929 (2008).
39. E. S. Schwartz, J. A. Christianson, X. Chen, J. H. La, B. M. Davis, K. M. Albers, G. F. Gebhart, Synergistic role of TRPV1 and TRPA1 in pancreatic pain and inflammation. *Gastroenterology* **140**, 1283–1291.e1-e2 (2011).
40. P. K. Randhawa, A. S. Jaggi, TRPV1 channels in cardiovascular system: A double edged sword? *Int. J. Cardiol.* **228**, 103–113 (2017).
41. V. Koko, J. Djordjeviæ, G. Cvijiæ, V. Davidoviæ, Effect of acute heat stress on rat adrenal glands: A morphological and stereological study. *J. Exp. Biol.* **207**, 4225–4230 (2004).
42. T. Ledowski, B. Bein, R. Hanss, A. Paris, W. Fudickar, J. Scholz, P. H. Tonner, Neuroendocrine stress response and heart rate variability: A comparison of total intravenous versus balanced anesthesia. *Anesth. Analg.* **101**, 1700–1705 (2005).
43. M. Meister, Physical limits to magnetogenetics. *eLife* **5**, e17210 (2016).
44. J. Landers, S. Salamon, H. Remmer, F. Ludwig, H. Wende, Simultaneous study of brownian and néel relaxation phenomena in ferrofluids by mössbauer spectroscopy. *Nano Lett.* **16**, 1150–1155 (2016).
45. D. J. Griffiths, in *Introduction to Electrodynamics,* D. J. Griffiths, Ed. (Cambridge Univ. Press, 2017), pp. 266–295.
46. C. D. Cox, C. Bae, L. Ziegler, S. Hartley, V. Nikolova-Krstevski, P. R. Rohde, C.-A. Ng, F. Sachs, P. A. Gottlieb, B. Martinac, Removal of the mechanoprotective influence of the cytoskeleton reveals PIEZO1 is gated by bilayer tension. *Nat. Commun.* **7**, 10366 (2016).

Acknowledgments

Funding: This work was funded in part by the DARPA ElectRx Program under D. Weber (HR0011-15-C-0155), the Bose Research Grant, and the NIH BRAIN Initiative (1R01MH111872). This work made use of the MIT MRSEC Shared Experimental Facilities under award number DMR-14-19807 from the NSF. D.R. is a recipient of the MIT-Technion Fellowship. A.W.S was funded by National Defense Science and Engineering Graduate (NDSEG) Fellowship, 32 CFR 168a. J.M. is a recipient of Samsung Scholarship. Methods of analysis and additional data are included in the Supplementary Materials. **Author contributions:** D.R., A.W.S., A.S.W., and P.A. designed the experiments and performed all analyses. D.R., J.M., and D.G. synthesized, functionalized, and characterized the NPs. D.R., A.W.S., and I.Y. performed in vivo and in vitro experiments. D.R. performed immunohistochemistry studies. G.V. contributed to heart rate analysis and injection map algorithms. F.K. and M.G.C. designed and assembled magnetic apparatuses. P.-H.C. and L.Y.M. contributed to analyses of in vivo data. All co-authors contributed to the writing of the manuscript. **Competing interests:** The authors declare that they have no competing interests. **Data and materials availability:** All data needed to evaluate the conclusions in the paper are present in the paper and/or the Supplementary Materials. Additional data related to this paper may be requested from the authors.

Submitted 3 September 2019
Accepted 17 January 2020
Published 10 April 2020
10.1126/sciadv.aaz3734

Citation: D. Rosenfeld, A. W. Senko, J. Moon, I. Yick, G. Varnavides, D. Gregureć, F. Koehler, P.-H. Chiang, M. G. Christiansen, L. Y. Maeng, A. S. Widge, P. Anikeeva, Transgene-free remote magnetothermal regulation of adrenal hormones. *Sci. Adv.* **6**, eaaz3734 (2020).